NIRS Methods of Specifying Carbon Ion Dose

Naruhiro Matsufuji*, Yuki Kase and Tatsuaki Kanai

Radiation Effect Research Team, Research Center for Charged Particle Therapy,
National Institute of Radiological Sciences

*Corresponding: matufuji@nirs.go.jp

1. Introduction

Many studies in the field of radiobiology have revealed that the clinical or biological effectiveness of heavy charged particles is a variable quantity. It results in that a physical dose is still a primary quantity to be controlled in carbon ion radiotherapy like as other conventional radiations, however, a kind of modification is indispensable for therapeutic purpose. Here, RBE is introduced as a tool to account for the modification. However, RBE depends on various physical parameters, as mentioned above. Primarily, RBE of a heavy ion beam gradually increases as the LET by the beam increases, reaches its maximum and then decreases. In addition, the RBE curve is known to show a different behavior for different ion species, fractionation schedules, or even dose levels. Even if these physical conditions are identical, RBE also varies as a function of biological parameters such as the type of tissue or cell, oxygenic conditions, endpoint of interest, and so on. The enormous complexity of the RBE determination hinders itself from being fully understood even at this moment. At HIMAC, unproven behaviors of factors such as dose dependency or tissue-specific response to carbon ions are kept constant in order to ascertain them from clinical outcomes.

2. Materials and Methods

At first, fragmentation of monoenergetic carbon ions in a patient' s body is estimated with a simulation code HIBRAC [1]. Dose-averaged LET value is deduced at each depth from the calculated LET spectra. HSG, cell line from human salivary grand tumor, was chosen as a representative of various cell lines due to its moderate radiosensitivity. Dose-survival relationships of the HSG to carbon ions of various incident energies are characterized with 2 parameters, α and β, by the LQ model. SOBP is designed to achieve flat survival probability (10%) on HSG entire SOBP region. Here, dose-averaging coefficients α and β are used for survival calculation at each depth regarding composition of the beam.

It is assumed that carbon beam is clinically equivalent to fast neutrons at the point where dose-averaged LET values is 80 keV/μm. Our enormous neutron therapy experience tells that neutron has clinical RBE of 3.0. Then, clinical RBE of carbon is also normalized to 3.0 at the point. Clinical SOBP shape is finally deduced by equally multiplying a fixed factor, the ratio between clinical- and biological RBE value at the point where dose-averaged LET is 80 keV/μm, to entire biological SOBP.

This scheme for the designing of clinical dose results in applying universal depth-dose distributions to all patients, independent of tumor type or dose level. The universal depth dose distributions are considered to be beneficial to clarify the clinical effectiveness of carbon ion radiotherapy through clinical trials when dose dependency or the difference of radiosensitivity among tumor type is not yet proven from the viewpoint that it contributes to reduce the number of free parameters. Fig. 1 schematically shows the method for determining the RBE at the center of the SOBP for clinical situations.

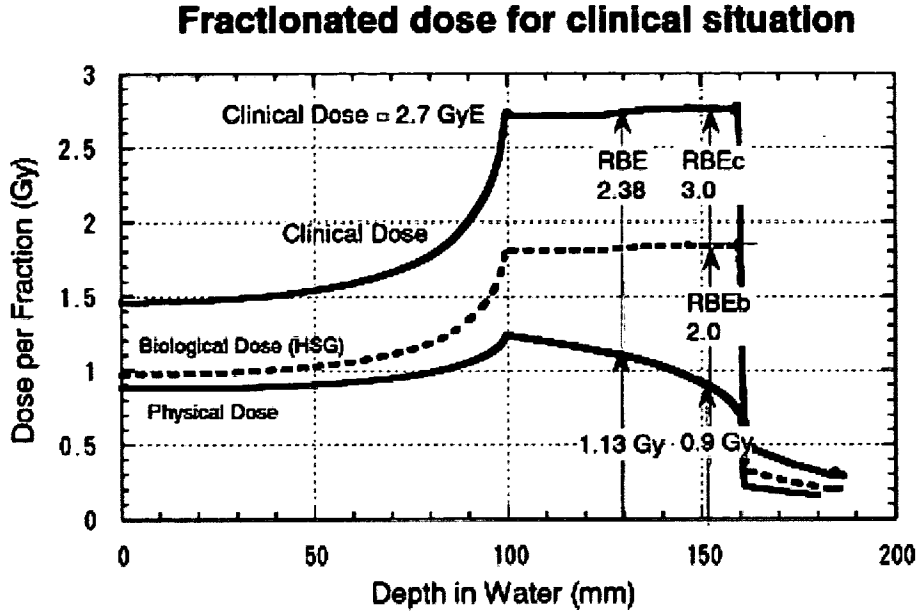

Fig. 1 Schematic method used to determine the RBE at the center of the SOBP for the clinical situation.

3. Results and Discussion

Verification of clinical RBE

We present here tumour control probability (TCP) analysis for non-small cell lung cancer (NSCLC) as an example of clinical results in terms of above-mentioned clinical RBE prescription scheme. Miyamoto et al. analyzed the clinical results of NSCLC treated by HIMAC beams [2]. They depict very conspicuous dose dependency of local control rate. The dose escalation study was performed with a treatment schedule of 18 fractions in 6 weeks. As to photon, Hayakawa el al. reported local control rate for NSCLC. In order to compare both results, the dose dependency of the TCP with the photon beam was fitted by the following formula [3];

$$TCP = \sum_i \frac{1}{\sqrt{2\pi}\sigma}\left\{-\frac{(\alpha_i-\alpha)^2}{2\sigma^2}\right\}\cdot\exp\left[-N\exp\left\{-n\alpha d\left(1+\frac{d}{\alpha/\beta}\right)+\frac{0.693(T-T_k)}{T_p}\right\}\right]. \quad (1)$$

α and β are coefficients of LQ model of cell survival curve. In the analysis, α and β values of HSG cells were used. σ is a standard deviation of the coefficient α, which reflects patient-to-patient variation of radiosensitivity. N is the number of clonogen in tumor (fixed value of 10^9 was used). n and d are total fraction number and fractionated dose, respectively. T (42 days), T_k (0 day) and T_p (60 days) are overall time for treatment, kick off time and average doubling time of tumor cells, respectively. Values used in the analysis are shown in brackets. The result is shown in fig. 2.

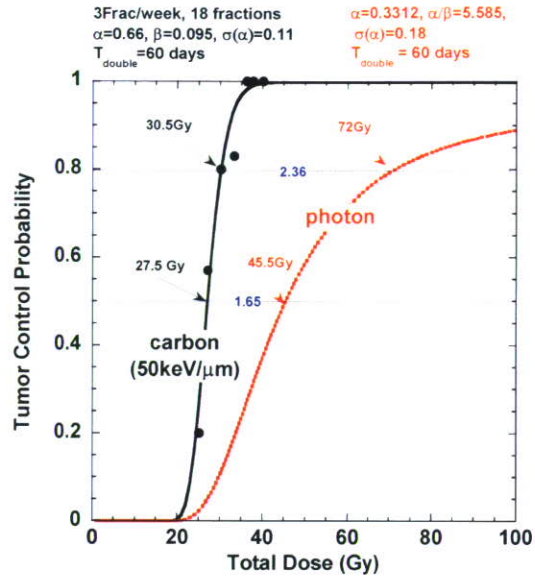

Fig. 2 TCP of NSCLC with photon (dashed, red line) and carbon (black line) beams. Circles show clinical result at HIMAC. For carbon TCP, width of SOBP and LET there were fixed as 60mm and 50 keV/μm, respectively.

Same analysis was carried out on the TCP with the carbon beam. Here, width of SOBP and dose-averaged LET in the SOBP region were both fixed as 60mm and 50 keV/μm, respectively for simplicity. The result is also shown in the figure. It is clear from the figure that the TCP curve of carbon beam is much steeper than that with photon beam. Values of s in eq. (1) is 0.18 for photon beam while for carbon beam, the value is reduced to 0.11. The result suggests that carbon beam provides equally excellent local tumor control irrelevant to individual radiosensitivity.

The difference of TCP slope shown in fig. 6 suggests that, when TCP is regarded as an endpoint, RBE value is dependent on the level of the TCP. It is found that our clinical RBE value corresponds to that at 80% TCP.

Application to hypofractionation

At HIMAC, hypofractionation study with carbon ions has been tried for some kind of tumors. Next to NSCLC, clinical trials on hepatomas will proceed into a single irradiation in no time. Before initiating a new protocol, it is desirable to estimate clinical results that correspond to prescribed dose level. The TCP analysis mentioned in the previous section is applied for this purpose. By applying σ value deduced from actual clinical result into eq. (1), it is possible to estimate TCP of different treatment schedule on NSCLC. This approach is adopted in the determination of the clinical dose to be prescribed for the single irradiation of hepatomas.

Comparison with GSI model

Different from our approach, GSI establishes and makes use of different approach named as Local Effect Model [4]. Resultant prescribed dose is apparently indicated in an identical unit GyE in both facilities; however, the value itself may differ due to the difference of the model. The difference of GyE at NIRS (GyE_{NIRS}) and GSI (GyE_{GSI}) is shown by converting GyE_{GSI} into GyE_{NIRS} in order to clarify required information on dose reporting.

An example of actual clinical dose distribution planned at GSI was converted into those by our scheme by the following steps.

(1) GSI clinical dose distribution (3.3GyE_{GSI} to chordoma with parallel opposing irradiation)

(2) Calculate three-dimensional dose-averaged LET and physical dose distribution with TRiP, an engine of treatment planning used at GSI.

(3) Calculate GyE_{NIRS} based on the physical information from (2).

The result is shown in fig. 3. It is found that GyE_{NIRS} is about 20% smaller than GyE_{GSI} for a typical 3.3GyE $_{GSI}$ treatment planning case.

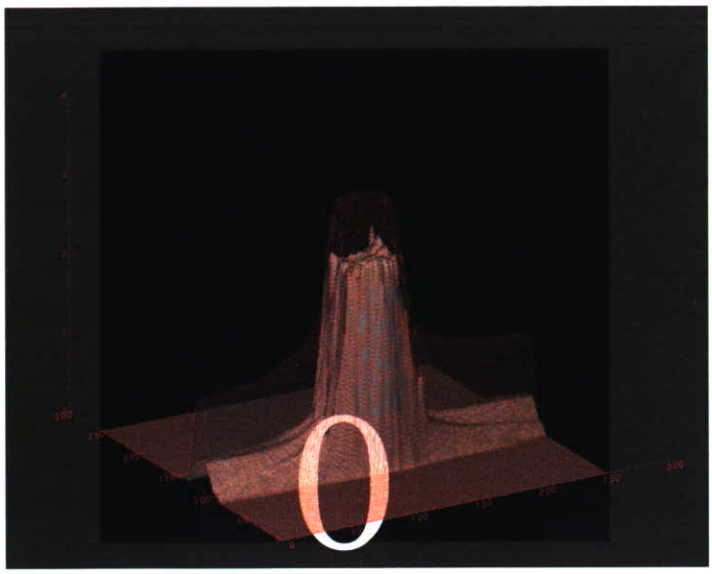

Fig. 3 Clinical dose distribution of GSI (red mesh) and NIRS (shade). The distribution was originally planned for the treatment of chordoma at GSI with parallel opposing field. At the target region, clinical GyE shows about 20% difference.

The difference is considered to be mainly due to the difference of biological system used in both model. The relationship will be affected by changing dose level, SOBP width, tumor site and so on. Hence it is too early to draw a conclusion from only one example, however, if we multiply a single factor 120% to the GSI' s physical dose distribution, the distribution agrees to ours in good precision at tumor region. Local control ratio of chordoma supports this assumption. It suggests the potential feasibility of converting GyE from one to another by multiplying single factor.

However, it is strongly required therefore to extend the comparison for various conditions and tabulate the conversion factor to make both clinical results totally comparable.

Estimation of clinical effectiveness

Currently a method has been developed in order to estimate the clinical dose from physical measurements. In this study, the microdosimetric spectra were measured with a spherical-walled proportional counter. The sensitive volume was filled with the propane-based tissue-equivalent gas from 0.5 to 6.0 micron in tissue-equivalent diameter in order to estimate the RBE value by the microdosimetric kinetic model (MKM) [5]. Actual RBE values of human tumor cells were obtained by colony assay, and compared with the model-estimated results. MKM is found to be capable of reproducing our clinical RBE values by introducing a correction that accounts for the overkill effect at high LET region [6].

4. Conclusion

Since 1994, more than 3,500 patients have been treated at HIMAC with the model explained in this paper. The design is found to be appropriate in contrast to the actual clinical indications.

The experience on the RBE intercomparison and the TCP analysis suggests that if the clinical results such as TCP or NTCP are expressed in terms of physical dose, it will provide good prospects to the clinical results such as the prospective estimation or the comparability among different facilities. From this point of view, it is pre-

ferable to report physical information (dose, LET and so on) together with the prescribed clinical dose. If appropriate simplifications can be introduced, the extent of physical information could be reduced.

5. References

1. Sihver, L., Tsao, C. H., Silberberg R, Barghouty, A. F. and Kanai, T. (1995) Calculations of depth-dose distributions, cross sections and momentum loss, Adv. Space Res. 17: 105-108.
2. Miyamoto, T., Yamamoto, N., Nishimura, H. et al. (2003) Carbon ion radiotherapy for stage I non-small cell lung cancer, Radiotherapy and Oncology 66:127-140.
3. Webb, S. and Nahum, A. E. (1993) A model for calculating tumour control probability in radiotherapy including the effects of inhomogeneous distributions of dose and clonogenic cell density, Phys. Med. Biol. 38: 653-666.
4. Scholz, M. in this proceedings.
5. Hawkins, R. ibid.
6. Kase, Y., Kanai, T., Matsufuji, N., et al. (2008) Biophysical calculation of cell survival probabilities using amorphous track structure models for heavy-ion irradiation, Phys. Med. Biol. 53, 37-59.

A Microdosimetric-Kinetic Model Relating Mammalian Cell Killing by Heavy Charged Particles to that of Gamma and X-rays

Roland Hawkins

Department of Radiation Oncology, Ochsner Medical Institutions, 1514 Jefferson Highway, New Orleans, Louisiana, 70121, USA

Corresponding: rhawkins@ochsner.org

INTRODUCTION

The relative biologic effectiveness (RBE) of ionizing radiation in causing the reproductive death of mammalian cells increases with increase in the linear energy transfer (LET) quality of the radiation. This property is an important consideration in determination of the schedule and dose when patients are treated with heavy charged particle radiation such as carbon ions. The microdosimetric-kinetic (MK) model (1,2) provides a relation between RBE in the limit of zero dose (RBE_1) and LET or, alternatively, between RBE_1 and a microdosimetric parameter equal to the dose average of the lineal energy spectrum (y_D) of the radiation (3). This relation is presented and its derivation from the MK model outlined. Experimental studies of the dependence of RBE_1 on radiation quality for several mammalian cell types (4-9) are examined in the context of the MK model. Some general relationships between cell killing by low and high LET radiation are suggested that may be useful in the selection of patients for treatment with high LET radiation and in the choice of dose and fractionation for such treatment.

SUMMARY OF THE MK MODEL

The cell nucleus is conceived of as divided into p compartments called domains. All domains have the same mass m but may have various shapes so that, as sketched in figure 1, they fill up the space of the nucleus like pieces in a three dimensional jigsaw puzzle. The energy deposited by exposure of a population of cells to ionizing radiation of macroscopically measured average dose D is actually concentrated along the paths of high

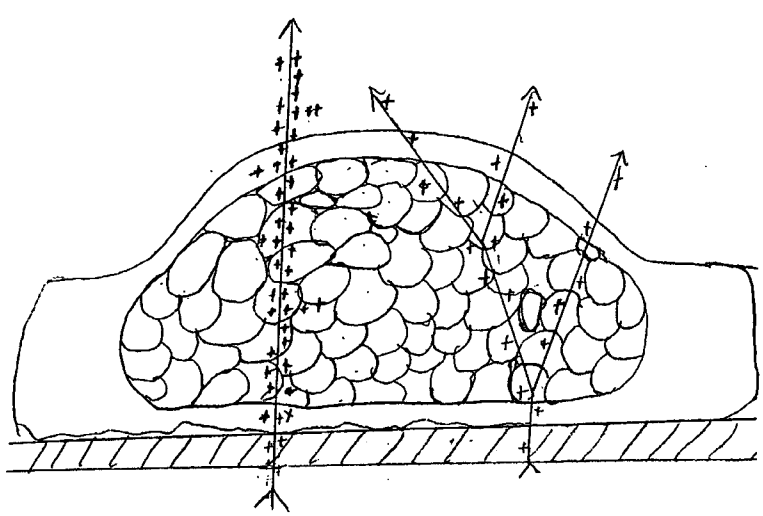

Figure 1: Nucleus of a cell spread on the surface of a culture dish and divided into compartments representing domains. On the left is sketched the track of a heavy charged particle of high LET. On the right is represented the track of a Compton electron produced by low LET X- or gamma rays.

energy charged particles of the radiation field, as depicted. As a result, the dose absorbed by individual domains varies from domain to domain and may be represented by a random variable called z. Note that $\langle z \rangle = D$ where the brackets indicate an average over all domains in the irradiated cell population.

It is further postulated that radiation induces potentially lethal lesions (PLL) in the DNA of the cell. The number of PLL in a domain is a random variable called x. The mass of DNA in a domain may also vary from domain to domain. It is a random variable called g. The value of x averaged over the subset of domains that absorb exactly z Gy and contain exactly g gm of DNA is assumed to be given by:

$$(1) \qquad \langle x | z, g \rangle = k_d z g$$

Where the brackets with bar indicate a conditional average and k_d is a proportionality constant. A PLL is a focus of chemical injury to the double stranded DNA where the strands may separate to form a double strand break. The value of k_d is estimated from measurements of the number of double strand breaks per cell per Gy, which is called k, where $k_d = k/p$. The value of k is about 30 to 40 per Gy per diploid human cell and is essentially the same for all mammalian cells and all values of LET up to at least about 100 $keV\,\mu m^{-1}$(10).

Figure 2 shows a single domain deformed to be a sphere of unit density, containing strands of DNA and with the path of a charged particle passing through it along a cord of the sphere. A number of PLL are shown marked on the DNA. The PLL are assumed to be confined to the domain in which they were created. They may wander about within the domain in a random flight, driven by thermal energy in a manner equivalent to Brownian motion. A pair of PLL may occasionally meet and interact to exchange strands to form what becomes a lethal exchange type of chromosome aberration. Only PLL formed in the same domain can do this. The concept of a domain incorporates in the MK model, in a simplified way, the notion that the chance of interaction between two PLL is greater the closer they are to one another. The domain acts as a surrogate for any of a number of possible restrictions on PLL travel. For instance, there may be membrane bound compartments in the nucleus or the DNA may be affixed to the nuclear membrane at multiple sites. Or, more likely, the distance a PLL on a DNA molecule can travel may be limited in a statistical sense by its half life before it disappears due to repair (11).

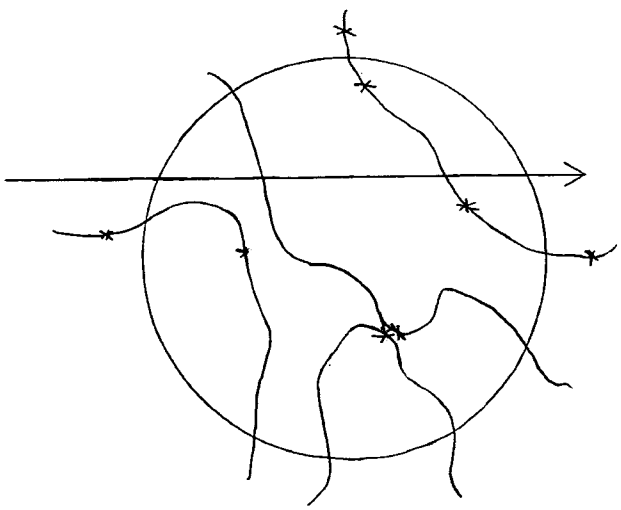

Figure 2: Sketch of a domain deformed into an equivalent sphere of the same mass and density of one gm per cm^3 and with the straight line path of a charged particle intersecting the domain along one of its cords. Also shown are parts of DNA strands from one or more chromosomes bearing marks representing radiation induced potentially lethal lesions.

The diameter of the sphere equivalent to a domain is called d. As demonstrated below, the value of d is in principle measurable and is a property of the cell. Its value has been found to be of the order of 0.5 to 1.0 micrometer for several cell types (table 1). The number of domains per nucleus is of the order of several hundred to a few thousand.

Let z_1 be a random variable equal to the dose imparted to a domain by passage of a single high energy particle through or near it. The distribution of z_1 is determined by the LET quality of the radiation and the size of the domain. Unlike z it does not depend on the dose D. An important quantity that contains the explicit dependence of survival on radiation quality is $\gamma = \langle z_1^2 \rangle / \langle z_1 \rangle$. It is estimated as the average length of a cord that intersects a spherical domain times the LET (1,2):

$$(2) \qquad \gamma \simeq \frac{3d}{4m} L = \frac{0.229}{d^2} L$$

Where d is the diameter of the domain equivalent sphere and L is the LET. Alternatively, it is given by:

$$(3) \qquad \gamma = \frac{4}{\pi d^2} y_D = \frac{0.203}{d^2} y_D$$

where the value of y_D is the dose weighted average of the distribution of the energy deposition events recorded in a spherical tissue equivalent proportional counter divided by the average length of a cord that intersects the counter. The effective counter diameter should be equal to or near that of a domain (3). The constants make the units be such that γ is in Gy if d is in μm and L and y_D are in $keV\mu m^{-1}$.

It is assumed that a PLL may undergo one of three processes. 1. It may be converted to a lethal unrepairable lesion via a first order monomolecular like process with rate constant a. For instance, this may be by separation of the DNA strand at the PLL to form two chromosome fragments that become a terminal deletion aberration and an acentric fragment. 2. As described above, it may combine with another PLL in the same domain to form a lethal unrepairable lesion with second order (bimolecular) rate constant b_d. 3. It may be repaired by a monomolecular-like process with rate constant c to restore the native chromosome continuity. Finally, if a PLL undergoes none of these three processes and instead persists for a time t_r, it converts to a lethal unrepairable lesion. Let the number of lethal lesions that form in a domain be a random variable called w_d. These specifications give rise to the mass action kinetic equations:

$$(4) \qquad \begin{aligned} \frac{d}{dt}\langle x|z,g\rangle &= -a\langle x|z,g\rangle - c\langle x|z,g\rangle - 2b_d\langle x|z,g\rangle^2 \\ &\approx -(a+c)\langle x|z,g\rangle \end{aligned}$$

$$(5) \qquad \frac{d}{dt}\langle w_d|z,g\rangle = a\langle x|z,g\rangle + b_d\langle x|z,g\rangle^2$$

Where the truncate approximation of equation 4 holds for dose $D \ll 150Gy$. The non linear term can be dropped because repair is by far the dominant process that eliminates PLL at doses low enough that $c\langle x \mid z, g\rangle \gg b_d\langle x \mid z, g\rangle^2$ (12). Solution of the pair of equations 4 and 5 for $\langle w_d \mid z, g\rangle$ using the truncate form of equation 4, then averaging over domains with all values of z and g and multiplying by the number of domains per cell gives a linear quadratic relation for the number of lethal lesions per cell (a random variable called w) averaged over all cells in a population instantaneously exposed to dose D(1,2).

(6) $$\langle w \rangle = \alpha D + \beta D^2 = (\alpha_0 + \gamma\beta) D + \beta D^2$$

The relations of the survival parameters to the kinetic constants are:

(7) $$\alpha_0 = \frac{ak}{(a+c)} + ke^{-(a+c)t_r} \quad \text{and} \quad \beta = \frac{bk^2}{2(a+c)} \frac{\langle g^2 \rangle}{\langle g \rangle^2}$$

The value of α_0 is the average number of lethal lesions per Gy per cell originating from a single PLL. The product βD is the average number of lethal lesions per Gy per cell originating from two PLL, each from a different particle track, when the dose is D. The product $\gamma\beta$ is the average number of lethal lesions per Gy per cell that originate from pair wise combination of PLL created by passage of a single charged particle though a cell.

If the lethal lesions are Poisson distributed among the cells of the population than equation 6 becomes the familiar linear quadratic relation for the fraction of cells S that survive dose D:

(8) $$-\ln S = \alpha D + \beta D^2$$

An expression for $RBE_l = \alpha/\alpha_R$ in which the subscript R indicates the value of α for the reference low LET radiation, usually 200 to 250 kVp X-rays or cobalt-60 radiation, can be written as:

(9) $$RBE_{lp} = \frac{\alpha_p}{\alpha_R} = \frac{\alpha_0 + \gamma\beta}{\alpha_R} = \frac{\alpha_0}{\alpha_R} + \frac{\beta}{\alpha_R} \frac{0.229}{d^2} L = \frac{\alpha_0}{\alpha_R} + \frac{\beta}{\alpha_R} \frac{0.203}{d^2} y_D$$

The subscript p is added to indicate the requirement for Poisson distribution of lethal lesions. Note that if α_0, β and d are independent of L and y_D, than RBE_{lp} is a straight line with slope proportional to β_R/α_R and d^2, and with intercept at zero LET or y_D equal to α_0/α_R. The ratio α_0/α_R is the fraction of lethal lesions originating from a single PLL for the reference radiation.

Particle tracks are Poisson distributed among the nuclei of the irradiated population. If passage of a single charged particle through a cell almost always causes zero or one lethal lesion and never, or hardly ever, causes two or more lethal lesions, the lethal lesions will also be Poisson distributed. As LET increases, the probability of two or more lethal lesions from a single particle passage increases. This causes grouping of lethal lesions in some cells to the exclusion and survival of others and causes RBE_l to deviate downward from the RBE_{lp} line. With the introduction of a parameter representing the cross sectional area the nucleus presents to the radiation beam, called σ, and assuming lethal lesion production continues to increase as indicated by equation 6 and implied by the line of equation 9, the MK model provides expressions that estimate α and RBE_l corrected for non Poisson distribution of lethal lesions (2). These are:

(10) $$\alpha = \frac{\left(1 - \exp\left[\frac{0.16\alpha_p L}{\sigma}\right]\right)}{\frac{0.16\alpha_p L}{\sigma}} \alpha_p = \frac{\left(1 - \exp\left[\frac{0.14\alpha_p y_D}{\sigma}\right]\right)}{\frac{0.14\alpha_p y_D}{\sigma}} \alpha_p$$

$$(11)\qquad RBE_1 = \frac{\alpha}{\alpha_R} = \frac{1-\exp\left(-\frac{0.16\alpha_P}{\sigma}L\right)}{\frac{0.16\alpha_P}{\sigma}L} RBE_{1p} = \frac{1-\exp\left(-\frac{0.14\alpha_P}{\sigma}y_D\right)}{\frac{0.14\alpha_P}{\sigma}y_D} RBE_{1p}$$

The values of RBE_{1p} and α_p are those that would be observed if, after lethal lesions are created per equation 6 they were to be magically redistributed individually and at random among the population of cells, ie, with Poisson distribution. The limiting forms of equation 11 are of interest:

$$(12)\qquad \lim_{L\to 0} RBE_1 = RBE_{1P} \quad \text{and} \quad \lim_{L\to\infty} RBE_1 = \frac{\sigma}{0.16\alpha_R}\frac{1}{L} = \frac{\sigma}{0.14\alpha_R}\frac{1}{y_D}$$

EXPERIMENTAL STUDIES OF RBE

Figures 3, 4 and 5 are some experiments that demonstrate the linear dependence of RBE_1 represented in equation 9 as well as the deviation from the line to form a maximum in RBE_1 as LET approaches about 100 $keV\mu m^{-1}$. Linearity implies constancy of β and the several model parameters on which it depends per equation 7. With the assumption that the production of lethal lesions continues to increase linearly as LET increases to values greater than those of the linear range and with a reasonable choice for the nuclear cross section, equation 11 may be made to fit experimental measurements of RBE_1 as it reaches and passes through the maximum that is found as LET increases to values greater than 100 $keV\mu m^{-1}$ (2). This implies the deviation from linearity that produces the maximum in RBE_1 is predominantly, if not entirely, due to the non Poisson distribution of lethal lesions and that production of lethal lesions actually does continue to increase linearly even though RBE_1 does not. Further, this implies the value of β and the constants on which it depends likely also do not change significantly as LET reaches and exceeds that of the maximum in RBE_1. Note that for LET low enough that lethal lesions are Poisson distributed, RBE_1 has no dependence on σ.

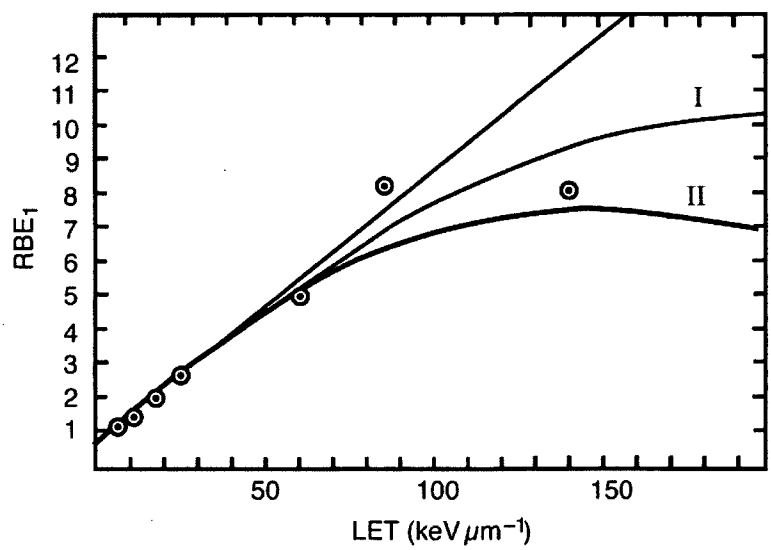

Figure 3: RBE_1 dependence on LET for unsynchronized human kidney cells. From data of reference 4 as plotted in reference 2. Reference radiation is 200 kVp X-rays. The straight line is equation 9, the parameters of which are listed in table 1. Curve I is equation 11 with $\sigma=100\mu m^2$ and Curve II with $\sigma=50\mu m^2$.

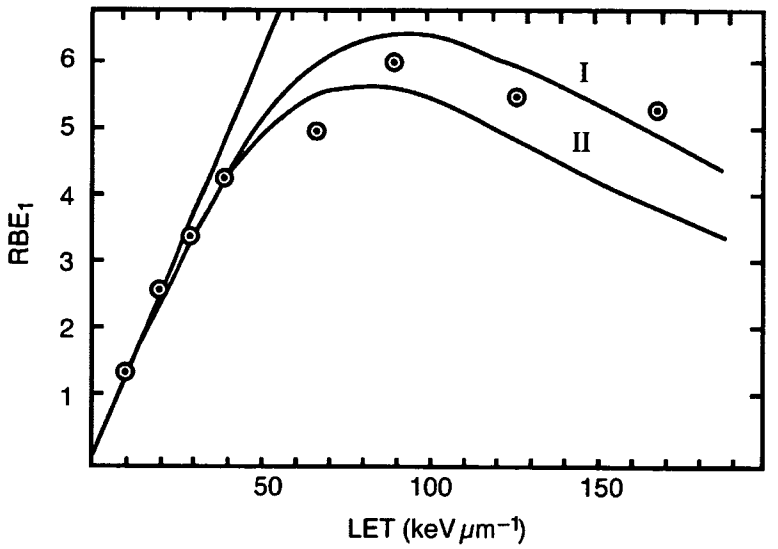

Figure 4: RBE_1 dependence on LET for V79 cells synchronized at G1/S transition. Data from reference 6, as plotted in reference 2. Reference radiation is 250 kVp X-rays. The straight line is equation 9, the parameters of which are listed in table 1. Curve I is equation 11 with $\sigma=32\mu m^2$ and curve II with $\sigma=24.6\mu m^2$.

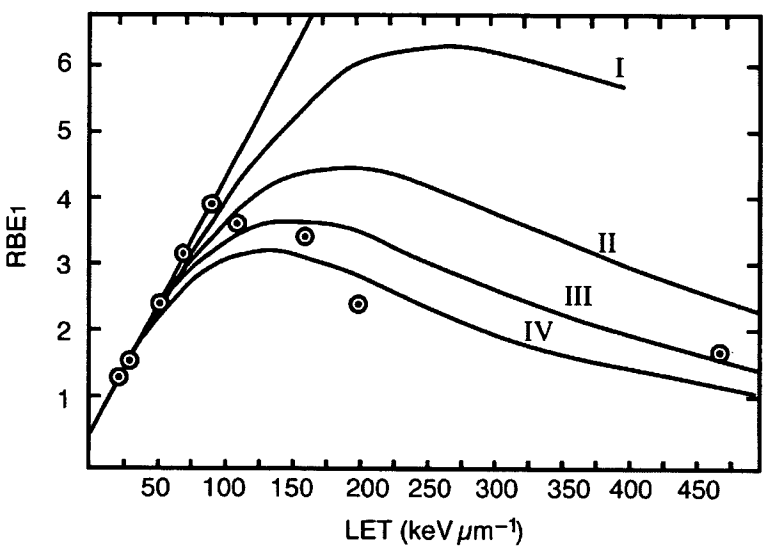

Figure 5: RBE_1 dependence on LET for unsynchronized HF-19 human diploid lung fibroblasts. Data from reference 5, as plotted in reference 2. Reference radiation is 250 kVp X-rays. The straight line is equation 9, the parameters of which are listed in table 1. Curve I is equation 11 with $\sigma=320\mu m^2$, curve II with $\sigma=160\mu m^2$, curve III with $\sigma=106.6\mu m^2$, curve IV with $\sigma=80\mu m^2$.

Figure 6 summarizes experimental determinations of the linear relation between RBE_1 and LET of equation 9 for the three cell types represented in figures 3,4 and 5 and additionally for fibroblasts obtained from patients who have the recessively inherited disease ataxia telangiectasia. All four lines are from least squares fit to data felt to be within the linear range of LET. There is uncertainty in their determination because the appropriate value of LET above which the data should be excluded because of deviation due to non Poisson distribution of lethal lesions is uncertain. This uncertainty affects the zero LET intercept more than it does the slope. By definition each line must pass through the RBE_1 equal one line at the LET of the reference low LET radiation, which is either 200 or 250 kVp X-rays. The appropriate value for the reference LET is uncertain. Accordingly the

RBE_1 equal one point was not included in the data used to determine the lines. The intersection of the lines with the RBE_1 equal one line suggests the reference radiation LET is in the range of about 3 to 10 $keV\mu m^{-1}$.

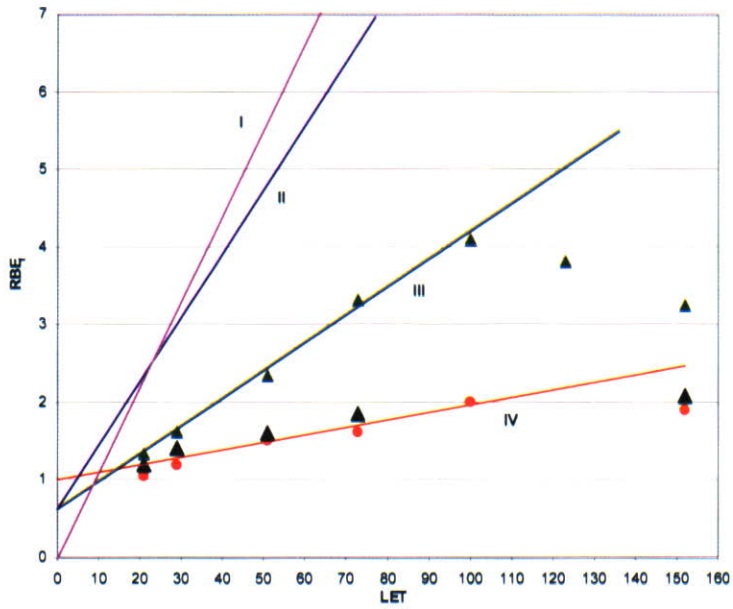

Figure 6: Composite for comparison of linear dependence of RBE_1 on LET per equation 9. Curve I is V79 cells from figure 4, II is human kidney cells from figure 3, III is HF-19 cells from figure 5, with data points shown. Line IV is fit to data for skin fibroblasts explanted from two patients with ataxia telangiectasia replotted from references 7 and 8. The reference radiation is 250 kVp X-rays.

Figure 7 shows a plot of data from Kase et al at NIRS (9) for two cell types using y_D as the measure of radiation quality. The value of y_D for the 200 kVp X-ray reference radiation has been measured with a tissue equivalent proportional counter with effective diameter of 0.76 and 0.97 micrometer. Its value is 4.3 $keV\mu m^{-1}$(9, 13)

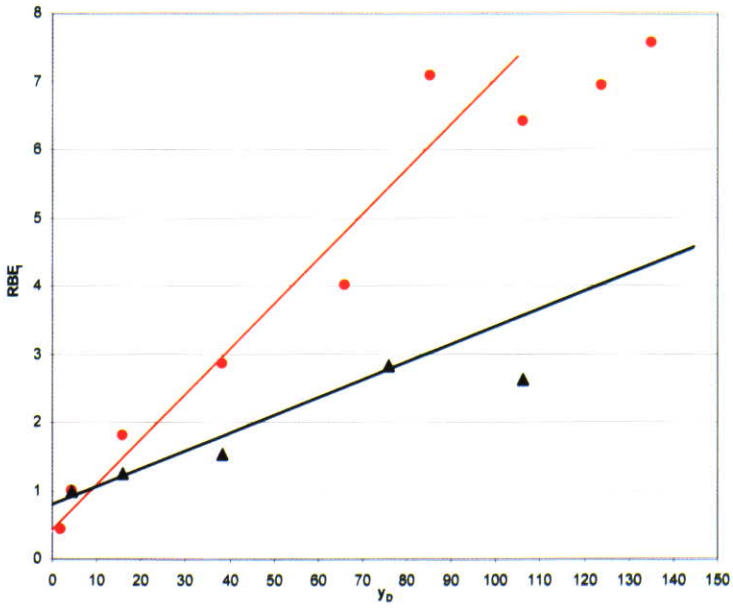

Figure 7: RBE_1 dependence on y_D. Plotted from data of reference 9. The steeper line is least squares fit to data for $y_D < 100 keV\mu m^2$ for human salivary gland cell line HSG and the less steep line similarly fit for normal human fibroblast strain GM05389. The lines represent equation 9, the parameters of which are listed in table 1.

and the RBE_1 equal one point is included in the data used to determine the lines in figure 7. Also included for the HSG cells is a point for cobalt 60 radiation for which y_D is 1.81 $keV\mu m^{-1}$(9). Measurements of RBE_1 for the lower end of the range of y_D are valuable as they particularly improve the accuracy of the determination of α_0/α_R. There is significant advantage in characterizing radiation quality by measurement of y_D rather than by LET.

DISCUSSION:

Table 1 summarizes parameters obtained from the linear relations shown in figures 6 and 7. The cells sort into three groups by the value of α_R. HSG, T-1 and V79 cells are immortalized cell lines able to be propagated indefinitely in culture. They form a relatively radioresistant group. HF-19 and GM05389 have been through a relatively low number of subculture passages and are expected to be able to undergo a limited number of future passages before senescence or death. They are diploid cells. They form a group of relatively radiosensitive cells with α_R about four times that of the established cell lines. The AT cells form an ultra-radiosensitive group with α_R about ten times that of the established cell lines.

Cell type references	AT	HF-19	GM05389	HSG	T-1	V79,G1/S
Charged particle	^3He	^3He	^{12}C	^{12}C	^1H ^4He	$^1H, ^2H$ ^3He
$\alpha_R\left(Gy^{-1}\right)$	2.5	0.80	0.70	0.19	0.19	0.234
$\beta_R\left(Gy^{-2}\right)$	----	----	-----	0.05	0.038	0.042
$\lim_{L\to 0} RBE_{1P} = \alpha_0/\alpha_R$	0.99	0.59	0.81	0.44	0.64	0.018
$\frac{dRBE_{1P}}{dL}$	0.0102	0.037	0.0251	0.0685	0.082	0.11
$\alpha_0\left(Gy^{-1}\right)$	2.4	0.47	0.57	0.084	0.12	0.0
$d(\mu m)$	(0.62)	(0.58)	(0.76)	0.89	0.75	0.61
$RBE_1(\max)$	2	4	3	7	8	6
$\alpha_{\max}\left(Gy^{-1}\right)$	5.0	3.2	2.1	1.33	1.52	1.40
$\frac{\beta}{d^2} = \frac{dRBE_{1P}}{dL}\frac{\alpha_R}{0.229}$	0.111	0.129	0.0865	0.0641	0.0680	0.112

Table 1: Summary of parameters of survival and of the line representing equation 9 for the various cell lines referred to in the figures.

Since the experimental measurement of RBE_1 versus LET or y_D indicates linear dependence, it is implied that β is constant and equal to β_R. The value of β_R is shown for the three established cell lines. There is not much variation in β_R among the three. It is not possible to reliably measure β_R for the more sensitive cell types and no value is listed for them. The survival relation for the sensitive cells, even for X-rays or cobalt-60 radiation, appears to be exponential, or nearly so. This is because the dominant effect of a large value of α_R for the dose range

accessible for colony survival measurements makes β_R appear to equal zero. However, it can not be zero because, if it were, there would be no increase in RBE with increasing LET.

Since there is little variation in β_R among cells for which it can be measured, the average of the three may serve as an estimate of β_R for the other cells. The average value of β_R for the three cell lines is 0.043 Gy^{-2}. Computation of the domain diameter d from the slope of the line of equation 9 requires a value for α_R and β_R, or at least their ratio. Computed values of d are listed in table 1. Those in parenthesis were computed with β_R set equal to the average value of 0.043 Gy^{-2}. The computed domain diameter values show little variation suggesting that a value of d equal to that of the average of those in table 1, which is 0.7 micrometers, may approximate that of many mammalian cells.

When sensitivity is expressed by the value of α_0 the cells sort into the same sensitivity groups as for α_R. Vulnerability to formation of a lethal lesion from a single PLL is apparently a major determinant of the magnitude of α_R. By increasing the value of α_R, a relatively large value of α_0 tends to make the ratio β_R/α_R low. Per equation 9, this leads to less increase in RBE_{1p} with increasing LET. This is confirmed by the entries for $dRBE_{1p}/dL$ in table 1.

The lower value of $dRBE_{1p}/dL$ leads to a lower maximum value of RBE_1, which is listed in table 1 as RBE_1 (max). This trend is not enough to reverse the order of sensitivity of the cell groups as judged by the maximum value attained by α, which is listed in table 1 as α_{max}. However, note that whereas α_R of the radiosensitive diploid human fibroblasts is about 4 times that of the established cell lines, α_{max} is only about 1.5 to 2 times that of the established cell lines. This suggests the generalization that as LET increases to approach that of the maximum in RBE_1, the ratio of α of more sensitive cell types to α of more resistant cell types becomes closer to one than it is for cobalt-60 or X-rays.

CONCLUSION:

Since the value of β_R shows relatively little variation among cells, the ratio β_R/α_R is largely determined by variation in the value of α_R, which in turn is largely determined by the vulnerability of the cells to formation of lethal lesions from single PLL, as expressed in the value of α_0. Since the rate of increase in RBE with LET is proportional to β_R/α_R, a relatively large value of α_R, and the radiosensitivity it represents, implies a lower maximum value of RBE for the more radiosensitive cells. This tends to reduce the differential in sensitivity between any pair of cell types as LET increases toward that of the maximum in RBE, as compared with the differential in sensitivity to high energy X-rays or cobalt 60. This may be particularly advantageous in treating cancers that are relatively radioresistant and in eradicating radioresistant subpopulations present in many tumors. Note for instance that the relative resistance of hypoxic cells expressed as the oxygen enhancement ratio tends to disappear as the LET approaches that of the maximum in RBE (14-16). This can be explained by the loss of Poisson distribution of lethal lesions (2).

Since α increases by several fold as LET increases up to the maximum in RBE, while β remains essentially unchanged, the α/β ratio also increases several fold. Because of this, unlike for high energy X-rays, there is essentially no sparing of cells of normal tissues by decreasing the fractional dose in a course of radiation treatment with high LET radiation. This is particularly important to recognize in treatment that must include the brain, spinal cord or other tissues for which the α/β ratio appropriate to low LET radiation is small (2 to 5) and which are relatively spared by small fractions of the high energy X-ray radiation used to treat patients in nearly all radiation oncology clinics.

REFERENCES

(1) R B Hawkins, A microdosimetric-kinetic theory of the dependence of the RBE for cell death on LET. Med. Phys. **25**, 1157-1170 (1998).

(2) R B Hawkins, A microdosimetric-kinetic model for the effect of non-Poissson distribution of lethal lesions on the variation of RBE with LET. Radiat. Res. **160**, 61-19 (2003).

(3) ICRU, Microdosimetry. Report 36, International Commission on Radiation units and Measurements, Appendix F, Bethesda MD, (1983).

(4) G W Barendsen, H M D Walter, J F Fowler and D K Bewley, Effects of different ionizing radiations on human cells in tissue culture III. Experiments with cyclotron-accelerated alpha-particles and deuterons. Radiat. Res. **18**, 106-119 (1963).

(5) R Cox and W K Masson, Mutation and inactivation of cultured mammalian cells exposed to beams of accelerated heavy ions III. Human diploid fibroblasts. Int. J. Radiat. Biol. **36**, 149-160 (1979).

(6) R P Bird, N Rohrig, R D kColvett, C R Geard, and S R Marino, Inactivation of synchronized Chinese hamster V79 cells with charged particle track segments. Radiat. Res. **82**, 277-289 (1980).

(7) R Cox, A cellular description of the repair defect in ataxia-telangiectasia. In: Ataxia-telangiectasia: A Cellular and Molecular Link Between Cancer, Neuropathology, and Immune Deficiency. Edited by: B A Bridges and D G Harnden (John Wiley and Sons, London), 141-153 (1982).

(8) D T Goodhead, J Thacker and R Cox, The effects of radiations of different qualities on cells: molecular mechanisms of damage and repair. Int. J. Radiat. Biol. **63**, 543-556 (1993).

(9) Y Kase, T Kanai, Y Matsumoto, Y Furusawa, H Okamoto, T Asaba, M Sakama and H Shinoda, Microdosimetric measurement and estimation of human cell survival for heavy-ion beams. Radiat. Res. **166**, 629-638 (2006).

(10) K M Prise, G Ahnstrom, M Belli, J Carlsson, D Frankenberg, J Kiefer, M Lobrich, B D Michael, J Nygren and B Sternerlow. A review of dsb induction data for varying quality of radiations. Int. J. Radiat. Biol. **74**, 173-184 (1998).

(11) R. Hawkins, A microdosimetric-kinetic model for the sensitization of V79 cells to radiation by incorporation of bromodeoxyuridine. Radiat. Res. **155**, 698-702 (2001).

(12) Hawkins, A microdosimetric-kinetic model of cell death from exposure to ionizing radiation of any LET, with experimental and clinical applications. Int. J. Radiat. Biol. **69**, 739-755 (1996).

(13) M Coppola, E Eickel, M Fitzgerald, D Pirwitz, F Porro and J Booz. Experimental evaluation of the spectral energy deposition in small volumes by low LET radiation. In Proceedings of the Fifth Symposium on Microdosimetry, Report No. EUR 5452. Edited by J Booz, H G Ebert and B G Smith. (Commission of the European Communities, Luxembourg) (1976).

(14) G W Barendsen and H M D Walter, Effects of different ionizing radiations on human cells in tissue culture. Radiat. Res. **22**, 314-329 (1964).

(15) E A Blakely, C A Tobias, T C H Yang et al, Inactivation of human kidney cells by high-energy monoenergetic heavy-ion beams. Radiat. Res. **80**, 122-160 (1979)

(16) Y Furusawa, K Fukutsu, M Aoki, et al, Inactivation o faerobic and hypoxic cells from three different cell lines by accelerated He-3, C-12 and Ne-20 beams. Radiat. Res. **154**, 485-496 (2000).

Treatment of Skull Base Chordomas at GSI

Daniela Schulz-Ertner MD[1,2], Christian P Karger PhD[3], Alexandra Feuerhakel, Anna Nikoghosyan MD[1], Stephanie E Combs MD[1], Oliver Jäkel PhD[3], Michael Scholz PhD[4], Jurgen Debus MD PhD[1]

[1]Dept. of Radiation Oncology, University of Heidelberg, Germany
[2]Dept of Radiation Oncology, Frankfurter Diakonie Kliniken, Frankfurt am Main, Germany
[3]Dept. of Medical Physics in Radiation Oncology, DKFZ, Heidelberg, Germany
[4]Dept. of Biophysics, Gesellschaft für Schwerionenforschung (GSI), Darmstadt, Germany

Corresponding : Daniela.Ertner@fdk.info

Abstract

Patients and Methods: Between November 1998 and July 2005, 96 patients with chordomas of the skull base have been treated with carbon ion RT using the raster scan technique at the Gesellschaft für Schwerionenforschung (GSI) in Darmstadt, Germany. All patients had gross residual tumors. Median total dose was 60 CGE (range 60 - 70 CGE) delivered in 20 fractions within 3 weeks. 44 Patients were treated within a clinical phase I/II trial between 1998 and 2001, and 52 further patients were treated thereafter as routine patients according to the same treatment protocol.

Results: Mean follow-up was 31 months (range 3 to 91 months). The actuarial local control rate was 70.0% at 5 years. Overall survival was 88.5% at 5 years. Late toxicity consisted of optic nerve neuropathy RTOG/EORTC grade 3 in 4.1% of the patients and necrosis of a fat plomb in one patient. Minor temporal lobe injury (RTOG/EORTC grade 1-2) occured in 7 patients (7.2%). Target doses in excess of 60 CGE and primary tumor status were associated with higher local control rates. A clear dose-reponse-relationship was observed when results were compared to other available data in the literature.

Conclusion: Carbon ion RT is an effective treatment option for skull base chordomas and is associated with acceptable toxicity. Doses in excess of 75 CGE with daily fractions of 2 CGE are likely to increase local control probability. A prospective phase III trial is needed to test the hypothesis that carbon ion RT is superior to proton RT with respect to toxicity at equieffective doses.

Introduction

Chordomas are rare tumors which are characterized by low radioresponsiveness. About 35% of all chordomas arise in the skull base region. Complete removal of skull base chordomas is challenging due to the close vicinity to sensitive normal brain structures. After incomplete tumor resection, postoperative RT is generally recommended. Since effective tumor doses in excess of 70 Gy can hardly be reached with photons, particle therapy with protons and carbon ions has been investigated in the past for these patients [1,2,3,4,5].

At GSI, patient treatments have been carried out within a cooperative project by medical doctors of the University of Heidelberg and scientists of the GSI, the German Cancer Research Center and the Research Center Rossendorf since 1997.

Here we report our experience with carbon ion RT in patients with skull base tumors. The focus of this article is on target definition and dose prescription using active beam delivery for carbon ion RT in skull base chordomas.

Material and Methods

Patients

First patients with skull base chordomas were treated with carbon ion RT at GSI in 1998. Since then, more than 150 patients with skull base chordomas have been treated with carbon ion RT at GSI. The first 44 chordoma patients were treated within a clinical phase I/II trial, the following patients were treated as routine patients according to the same protocol. The most recent analysis of treatment results in skull base chordomas treated at GSI has been performed in 2006 and included 96 patients with macroscopic chordomas of the skull base. There were 54 male and 42 female patients. The median age was 47 years (range 11-80 years). Fifty-nine patients (61%) were treated for primary tumors and 37 patients had recurrent tumors. All patients had macroscopic tumors when carbon ion RT was initiated. The average follow-up period at the timepoint of the last analysis was 31 months (range 3-91 months). For detailed information on patient characteristics see Schulz-Ertner et al. [4]

Target definition and treatment planning

Patients with skull base chordomas treated with carbon ion RT at GSI were positioned within a precision head mask and target localization was performed using stereotactic methods. The used immobilization device guarantees an accuracy of 1-2 mm [6]. The initial planning target volume (PTV1) included the gross tumor volume (GTV) plus a safety margin of 1-5mm to account for suspected subclinical disease based on clinical risk estimation. Surgical and histological reports, MRI findings and normal tissue constraints were taken into account. Even for very small tumors the entire clivus and the prevertebral muscles down to the basis of the second cervical spine were included into PTV1. Implantation metastases of skull base chordomas are reported in the literature, but the incidence of implantation metastases within the surgical pathway is reported to be as low as 5 to 10% [7,8]. Therefore, no efforts were made to completely cover the surgical pathway, thus avoiding unacceptable toxicity.

The PTV2 was defined to include the gross tumor volume (GTV) visible on the treatment planning MRI. A safety margin of 1-2mm was added to account for any movements and uncertainties in the set-up throughout the treatment course. The needed safety margin depends on the used immobilization device and was determined to be 1-2mm for the skull base region when rigid precision head masks were used. The delineation of target volumes and organs at risk was done on treatment planning CT images and coregistered MRI images according to the ICRU 50 and ICRU 62 recommendations for conformal RT. T2 weighted fat saturated and post gadolinium T1 weighted MRI sequences were found most adequate to separate the tumor accurately from normal tissues in the skull base region.

Carbon ion beams were delivered actively to the tumor using the raster scan technique [9]. Plan optimization included biologic plan optimization taking into account the local RBE (relative biological effectiveness) values. Plan optimization aimed at achieving a homogenous biologically effective dose throughout the target volume. The mean RBE for our patients was about 3 within the target volume. The local effect model (LEM), which is integrated in the TRiP software to calculate the RBE at each point, has been described in detail by Scholz et al. [10].

Dose prescription

Target dose was prescribed to each voxel of the target volume necessitating optimization of the absorbed dose in such a way that the product of the absorbed dose and the calculated local RBE value at each voxel was the

biologically effective prescription dose. The biologically effective dose was prescribed to every scan spot throughout the dose distribution. The allowed deviances between measured and prescribed doses were kept below 5% of the prescribed dose at each point. Treatment planning aimed at covering target volumes by the 90%-isodose line and underdosage was avoided within the target volume. Dose-volume-histogram data was generated for the physical and the biologically effective dose distributions for the planning target volumes and organs at risk. PTV1 was treated to target doses between 45 and 52.5 CGE within 15 fractions. A boost dose of 15 to 17.5 CGE was delivered to the PTV2, the total target dose reached within PTV2 was therefore 60 to 70 CGE. Eighty-four patients received a target dose of 60 CGE, higher doses up to 70 CGE were delivered in 12 patients.

Late toxicity to normal brain tissue such as necrosis is assumed to be the dose limiting toxicity for radiation therapy of skull base chordomas. An α/β value of 2-3 Gy can be estimated for the biological endpoint brain necrosis. An α/β value of 2 Gy was chosen for biological plan optimization. The α/β ratio for chordoma cells is not known, but from their biological behaviour with slow tumor progression and low radioresponsiveness it can be concluded that it is also in the range of 2 Gy.

A fractionation of 7 x 3.0 to 3.5 CGE per week was applied. Using a conventional fractionation scheme of 2 CGE per day and conservatively assuming an α/β of 2 Gy for late toxicity to the brain tissue and chordoma cells, biologically equivalent doses (BED) between 75 and 96.25 CGE were reached in PTV2. The doses to optic nerves and optic chiasm were restricted to 54 CGE. The accepted maximum dose to the brainstem was 50 CGE at the center, while very small volumes of less than 1mL at the surface of the brainstem were allowed to receive up to 60 CGE. The dose to the spinal cord was constrained to 45 CGE. Taking into account the accelerated fractionation pattern used for carbon ion RT at GSI, biologically equivalent dose constraints were 63.45 CGE for optic nerves and chiasm, and 75 / 56.25 CGE for the surface / center of the brain stem, respectively. These dose constraints were similar to the dose constraints adhered to in most of the proton centers. Therefore, similar toxicity rates can be expected.

Results

Twenty-one patients (21.8%) showed partial remission of their tumors on follow-up MRI scans after carbon ion radiation therapy. The local control rate was 70% at 5 years. Most recurrences were located inside the former RT field. Delivery of target doses exceeding 60 CGE improved local control significantly as well as primary tumor status, while gender did not influence outcome. Three percent of the patients developed implantation metastases within the surgical pathway outside the former carbon ion RT portals. Two patients (2%) developed distant metastases. The 5-year overall survival rate was 88.5%.

Carbon ion RT was well tolerated by most of the patients. Optic nerve neuropathy RTOG/EORTC grade 3 occured in 4 patients (4.1%). Circumscribed white matter changes in the temporal lobe occurred in 7 patients (7.2%) and were much more common in patients who received target doses in excess of 60 CGE (biologically equivalent doses between 75 and 96.25 CGE). In patients who received a total dose of 60 CGE (biologically equivalent dose of 75 CGE) the temporal lobe injury rate was 3.5%. A rate of 33% was observed in patients who received doses in excess of 60 CGE. The temporal lobe lesions were associated with a perifocal edema and neurologic sequelae necessitating steroid medication (RTOG/EORTC grade 2) in 2 patients, only. The remaining 5 patients were asymptomatic and the white matter changes were reversible (RTOG/EORTC grade 1) in these patients. Soft tissue necrosis of a fat plomb inserted into the surgical pathway during surgery was observed in one patient (RTOG/EORTC grade 3).

More detailed data on outcome and toxicity can be found in Schulz-Ertner et al. [4].

Discussion

The oncological problem in skull base chordomas is mainly a local problem. In our carbon ion RT patient series, 11 out of 15 locoregional recurrences occured inside the former RT fields, only 4 patients developed marginal failures. No patient developed an out of field recurrence. This supports the adequateness of the target volume concept.

Distant metastases are uncommon. Incidence rates between 0 and 14% have been reported [5,7,11].This is in line with the distant metastases rate of 2% found in our series.

There is no doubt that local control is dependent on the delivery of high local doses in skull base chordomas. Particles such as protons and carbon ions offer advantages in escalating doses to circumscribed tumors while avoiding dose to critical organ structures nearby. Based on these facts, high dose proton RT has been investigated in chordomas of the skull base in the past.

Munzenrider et al. achieved a 5-year local control rate of 73% in 375 patients treated with proton RT at the Massachusetts General Hospital in Boston, USA [3].

Hug et al. report a local control rate of 59% for chordoma patients treated with protons at Loma Linda University Medical Center, USA [2].

At the Centre de Protontherapie d' Orsay, France, patients with skull base chordomas have been treated with combined photon and proton RT to doses between 67 and 71 CGE. The 4-year local control rate was 53.8% [1].

The 5-year local control rate of 70% obtained with carbon ions at GSI is somewhat higher [4], but compares favourably with the data obtained in some of the proton series with prescription doses of at least 74 CGE. The data collected at GSI as well as the data available in the literature clearly supports the assumption that particle therapy is beneficial for patients with skull base chordomas, since much lower local control rates are reported for photon RT. After conventional photon RT local control rates between 17 and 23% at 5 years have been reported [12,13]. A clear dose-response-relationship has been described for skull base chordomas taking into account all these data [4]. In congruence with this finding, prescription dose has been identified as most important prognostic factor [1,14]. Higher doses are likely to achieve higher local control rates. Strategies of combining photons and particles can therefore be considered less favourable. Highest tumor doses are reached with protons or carbon ion RT alone, because the achieved dose gradients are much steeper than with photons due to the physical properties of proton beams. Biological equivalent target doses of at least 75 CGE are recommended. Using carbon ion RT, escalation of the biological equivalent target dose to doses in excess of 75 CGE seems to be feasible in patients with small tumors in uncritical location. However, one has to be aware that the risk for temporal lobe injury will increase with higher target doses as well.

After carbon ion RT, a higher local control rate was achieved in patients with primary tumor status as compared with patients treated for recurrent tumors. Primary tumor status has been considered to be an important prognostic factor as well by others [11,15].

Female gender was found to be an unfavourable prognostic factor after proton RT in skull base chordomas [14,16]. In our series, local control and overall survival rates did not significantly differ with respect to gender.

As compared to protons, carbon ions offer the possibility to reduce overall treatment time. The overall treatment time can be reduced to 3 weeks without increasing acute and late toxicity. Acute toxicity is very mild and severe late toxicity to optic nerves and chiasm occured in 4.1% of all patients treated with carbon ion RT at GSI, only. This rate compares to the best proton series.

Conclusions

Carbon ion RT has been proven to be an effective treatment option for skull base chordomas with respect to local control and overall survival. Carbon ion RT minimizes severe side effects to neighboring normal tissue structures. A prospective phase III trial is needed to test the hypothesis that carbon ion RT is superior to proton RT with respect to toxicity at equieffective doses.

References

Noel G, Feuvret L, Calugaru V, et al. (2005) Chordomas of the base of the skull and upper cervical spine. One hundred patients irradiated by a 3D conformal technique combining photon and proton beams. Acta Oncologica 44: 700-708.

Hug EB, Loredo LN, Slater JD, et al. (1999) Proton radiation therapy for chordomas and chondrosarcomas of the skull base. J Neurosurg 91(3): 432-439.

Munzenrider JE, Liebsch NJ (1999) Proton therapy for tumors of the skull base. Strahlenther Onkol 175 (Suppl 2): 57-63.

Schulz-Ertner D, Karger CP, Feuerhake A, et al (2007) Effectiveness of carbon ion radiotherapy in the treatment of skull-base chordomas. Int J Radiat Oncol Biol Phys 68(2): 449-457.

Weber DC, Rutz HP, Pedroni ES, et al. (2005) Results of spot-scanning proton radiation therapy for chordoma and chondrosarcoma of the skull base: the Paul Scherrer Institut experience. Int J Radiat Oncol Biol Phys 63(2): 401-409.

Karger CP, Jäkel O, Debus J, et al. (2001) Three dimensional accuracy and interfractinoal reproducibility of patient fixation using a stereotactic head mask system. Int J Radiat Oncol Biol Phys 49: 1493-1504.

Fagundes MA, Hug EB, Liebsch NJ, et al. (1995) Radiation therapy for chordomas of the base of skull and cervical spine: pattterns of failure and outcome after relapse. Int J Radiat Oncol Biol Phys 33(3): 579-584.

Austin JP, Urie MM, Cardenosa G, Munzenrider JE (1993) Probable causes of recurrence in patients with chordoma and chondrosarcoma of the base of skull and cervical spine. Int J Radiat Oncol Biol Phys 25 : 439-444.

Haberer T, Becher W, Schardt D, et al. (1993) Magnetic scanning system for heavy ion therapy. Nucl Instr Meth Phys Res 330: 296-305.

Scholz M, Kellerer AM, Kraft-Weyrather W (1997) Computation of cell survival in heavy ion beams for therapy. The model and its approximation. Radiat Environ Biophys 36: 59-66.

Hug EB, Fitzek MM, Liebsch NJ, et al (1995) Locally challenging osteo- and chondrogenic tumors of the axial skeleton: results of combined proton and photon radiation therapy using three-dimensional treatment planning. Int J Radiat Oncol Biol Phys 31(3): 467-476.

Magrini SM, Papi MG, Marletta F, et al. (1992) Chordoma ? natural history, treatment and prognosis. Acta Oncologica 31(8): 847-851.

Romero J, Cardenes H, la Torre A, et al. (1993) Chordoma: Results of radiation therapy in eighteen patients. Radiother Oncol 29: 27-32.

Terahara A, Niermierko A, Goitein M, et al (1999) Analysis of the relationsship between tumor dose inhomogeneity and local control in patients with skull base chordoma. Int J Radiat Oncol Biol Phys 45(2) : 351-358.

Gay E, Sekhar LN, Rubinstein E, et al. (1995) Chordomas and chondrosarcomas of the cranial base: results and follow-up of 60 patients. Neurosurgery 36(5): 887-896.